

Sol-gel synthesis and characterization of $\text{MgCO}_3 - \text{Al}_2\text{O}_3$ composite solid electrolytes

M. Sulaiman^{a,*}, M. F. Z. Kadir^b, A. N. Che Mat^c

^aChemistry Division, Centre for Foundation Studies in Science, University of Malaya, 50603 Kuala Lumpur, Malaysia.

^bPhysics Division, Centre for Foundation Studies in Science, University of Malaya, 50603 Kuala Lumpur, Malaysia.

^cDepartment of Chemistry, Faculty of Science, University of Malaya, 50603 Kuala Lumpur, Malaysia.

Corresponding Author Email: mazdid@um.edu.my

ABSTRACT

Composite solid electrolytes in the system $(1-x)\text{MgCO}_3 - x\text{Al}_2\text{O}_3$ with $x = 0.1 - 0.9$ were synthesized by a sol-gel method and analyzed by X-ray diffraction, differential scanning calorimetry, thermogravimetric analysis, scanning electron microscopy, energy dispersive X-ray, Fourier transform infrared spectroscopy and alternating current impedance spectroscopy for the determination of the phases and crystallinity, thermal stability, surface morphology, elemental composition, chemical bonding and conductivity, respectively. The composites show that, the crystallinity of the composites decreases as the amount of Al_2O_3 increase which could lead to higher conductivity. The thermal decomposition studies also indicate that the melting and/or decomposition of the composites occur at lower temperature than the pure MgCO_3 which normally take place at 350 °C. The composite with the ratio of $x = 0.9$ give the highest conductivity value in order of $10^{-4} \text{ S.cm}^{-1}$ as compared to other ratio due to effective transfer of charge carriers in addition to the formation of MgO-Mg^{2+} species at the interface.

Received: October-26-2020, Accepted: May-05-2021, <https://doi.org/10.14447/jnmes.v24i3.a05>

1. INTRODUCTION

High energy demand and climate change due to extensively burning fossil fuel had forced the researchers around the globe towards green energy generation mostly focusing on electrochemical energy conversions and storage. Research in multivalent battery such as magnesium (Mg) ion battery is indeed an utmost imperative in fuelling electric vehicles and most of the portable devices although it is still at the commencement stage [1]. However, investigation in battery is not as easy as projected. Numerous criterions need to be taken into account such as naturally abundance, cheap, less toxic towards the environment, possesses high energy and power density, long life cycle and enable to work in a wide range of temperature.

According to the recent report, investigation on Mg ion battery contribute about 80% of the literature from 1985 – 2015 [2]. The awareness for Mg battery lies on the fact that Mg has low reduction potential which is about -2.37 V versus normal hydrogen electrode (NHE) as well as high volumetric capacity (3866 mA cm^{-3}) which is almost double the value of Li ion battery (2046 mA cm^{-3}) [3, 4]. The research interest in our group is mainly on the development of solid composite electrolyte for Mg ion battery due to its better performance against the liquid electrolyte in terms of operating temperature, battery durability and safety [5]. There is no doubt that the first developed and the benchmark of solid composite electrolyte was $\text{Li}_x\text{PO}_y\text{N}_z$ in 1992 [6, 7] due to excellent electrochemical performance in terms of broad electrochemical window ranging from 0 – 5.5 V vs Li^+/Li . However, low ionic conductivity ($10^{-6} \text{ S cm}^{-1}$) and mechanical strength are the major apprehension apropos this type of solid electrolyte. Moreover, in terms of commercialization, magnesium ion battery is still at the beginning stage. Slow magnesium intercalation and/or diffusion into cathode as well as

irreconcilability between anode and electrolyte due to high overpotential (polarizing ability) of Mg^{2+} are some major issues that should be taken into consideration for practical purposes [8, 9].

Optimization of the ionic conductivity is undeniably a vital essential for solid composite electrolyte which deals closely with the preparation of the materials. Precipitation reaction [10], solid-state reaction [11], exchange reaction [12], sol-gel reaction [13], to name a few are among synthetic methods that have been explored to fabricate the solid composite electrolyte. Through a cautious control on the experimental conditions, the formation of porous nanoparticles with large specific surface area is the most desirable where the interconnection and/or the interfaces between the insulator and ionic conductor are prominently heightened which could enhanced the conductivity of solid composite electrolyte [14]. This phenomenon has been recounted hitherto by several authors who demonstrated that sol-gel technique could be able to deliver the homogeneous dispersion of the insulator into the ionic host conductor which promote better ionic conductivity of the electrolyte [15, 16].

To the best of the author's knowledge, there is no report in the literature regarding the preparation of $(1-x)\text{MgCO}_3 - x\text{Al}_2\text{O}_3$ with $x = 0.1 - 0.6$ based solid composite electrolyte. The existence of CO_3^{2-} anion is expected to enhance the ionic conductivity through disorientation of the anion as discussed from our previous study [5]. The as-prepared material is characterized by X-ray diffraction (XRD), Fourier Transform Infrared (FTIR), thermogravimetric analysis (TGA) and differential scanning calorimetry (DSC), Field Emission Scanning Electron Microscope-Energy Dispersive X-ray (FESEM-EDX) and electrochemical impedance spectroscopy for the determination of crystallinity and phases, chemical

bonding, thermal stability, surface morphology and ionic conductivity, correspondingly.

2. EXPERIMENTAL

2.1 Sample Preparation

Composite solid electrolytes in the system $(1-x)\text{MgCO}_3-x\text{Al}_2\text{O}_3$ with $x = 0.1 - 0.9$ mole were synthesized by a sol-gel method. MgCO_3 (purity > 99.0%, Fluka) and Al_2O_3 (purity > 99.7%, Sigma Aldrich) were used as purchased without further purification. First, a desired mole of MgCO_3 and Al_2O_3 were mixed in ethanol under magnetic stirring at room temperature. An equivalent amount of citric acid to the mass of Al_2O_3 was introduced to the solution after 10 min of stirring. Next, the solution was refluxed under magnetic stirring at 80 °C for several hours, followed by a drying process in a controlled oven at 120 °C for overnight. The powder was then ground in an agate mortar into a fine powder. In the final step, the powder was calcined at 900 °C in a furnace for 2 h. The sample was stored in a desiccator until conductivity measurement.

2.2 Characterization techniques

Structural characterizations for XRD and FTIR were performed on a PANanalytical EMPYREAN diffractometer with CuK_α radiation, $\lambda = 1.5406 \text{ \AA}$ and a Perkin Elmer Frontier spectrometer with 4 cm^{-1} resolution, respectively. The XRD data was obtained using X'Pert HighScorePlus software. The morphology and chemical content of the samples (pellets) were analyzed using FESEM-EDX SU8220 Hitachi. The thermal properties of the samples were measured on a Perkin-Elmer Pyris Diamond TG/DTA thermal analyzer in nitrogen atmosphere at a constant heating rate $5 \text{ }^\circ\text{C min}^{-1}$ at temperatures ranging from 30 to 900 °C. The DSC was obtained from the temperature range of 35–300 °C by Perkin-Elmer DSC 6 with a scan rate of $10 \text{ }^\circ\text{C min}^{-1}$. For conductivity studies, pellets were made by pressing the composite powders at a pressure of 9–10 tones cm^{-2} at room temperature. The diameter of the pellet was 13 mm and its thickness was about 1.1 mm. Conductivities were measured on a PGSTAT30 Autolab potentiostat/galvanostat (Ecochemie, Netherlands) impedance analyzer at frequencies ranging from $10^{-1} - 10^7 \text{ Hz}$ with an a.c amplitude of 100 mV. The conductivity measurements were conducted by sandwiching composite pellet between two stainless steel electrodes at temperatures ranging from room temperature to 150 °C.

3. RESULTS AND DISCUSSION

3.1 XRD analysis

The crystallinity of the materials was investigated by XRD as shown in **Fig.1** below. The XRD pattern for almost all ratios demonstrated about similar pattern where the formation of MgO can be observed at $2\theta = 36.5^\circ, 42.9^\circ$ and 62.5° which are in good agreement with the previous study [5, 17]. Meanwhile, Al_2O_3 was positioned at 2θ of $32.3^\circ, 39.5^\circ, 45.2^\circ, 60.3^\circ, 66.8^\circ$ as indicated recently [18–20]. The absence of MgCO_3 from XRD analysis indicative of complete conversion to MgO during the calcination process and the occurrence of the crystalline and amorphous phase of the prepared materials. This observation is in agreement with our previous experience in fabrication $\text{LiNO}_3\text{-Al}_2\text{O}_3$ composite where there was an

absence of LiNO_3 peak can be detected from XRD analysis [21, 22]. From Figure 1, the XRD analysis of the materials showed that the crystallinity increases as the amount of Al_2O_3 increased. The increments of the amorphousness of the composites give rise to the higher conductivity of the material. Furthermore, nanometer size of dispersoid which act as filler, where in the current work the filler is Al_2O_3 , prevent agglomeration thus enhancing the conductivity of the composite [23]. This finding is in parallel with Joge et al. [24] where they found that the conductivity reduced significantly as the crystallinity of the polymer electrolyte increased when the amount of Al_2O_3 increased to maximum of 6 wt%.

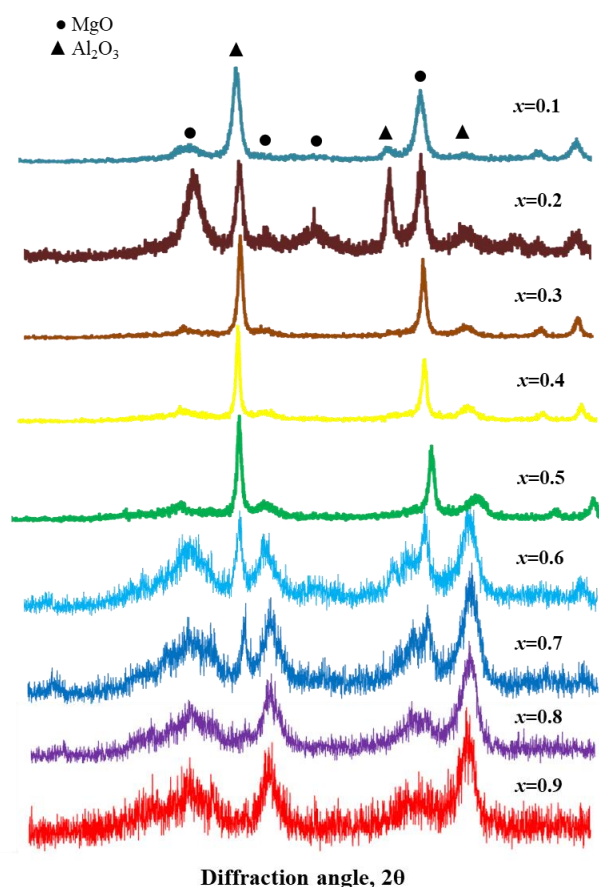


Figure 1: XRD patterns of Al_2O_3 and $(1-x)\text{MgCO}_3-x\text{Al}_2\text{O}_3$ composites.

3.2 DSC and TGA analyses

The thermal stability of the as-prepared materials were investigated by using DSC and TGA as demonstrated in Figure 2 and Figure 3, correspondingly. Typically, from the DSC analysis (Figure 2), the decomposition of adsorbed water ensue around 100 °C followed by the degradation of citric acid about the temperature of 140 °C until 170 °C [22]. However, as the temperature increased up to more than 250 °C, another endothermic peak due to the decomposition of MgCO_3 [25]. The melting point of the composites are lower than the melting point of MgCO_3 which normally occur at 350 °C indicative of local structural change phenomenon through disorder rearrangement when alumina was added into the composites which is supported by the previous studies where the decomposition temperature or the melting point of PEG-

$Mg(CH_3COO)_2 - CeO_2$ composites are much lower than pure PEG after the introduction of cerium oxide [26]. To support the DSC analysis, TG analysis has been conducted and almost all samples underwent three decomposition phase or region namely the dehydration and decomposition of citric acid, decomposition of $MgCO_3$ and the formation of MgO as validated in Figure 3. The weight loss of the as-prepared materials in region I from TG analysis was due to the dehydration process of the adsorbed water followed by the degradation of citric acid where the reaction took place up to the temperature of less than 200 °C. Nevertheless, as the temperature increased to more than 200 °C, $MgCO_3$ started to decompose (Region II) until it became stable at the temperature beyond 425 °C (Region III) where the formation of MgO can be obtained. It is noteworthy to mentioned that Region II from TG analysis where the application of temperature is more than 200 °C is the most crucial part in order to break the ionic bonding of $MgCO_3$ to produce mobile Mg^{2+} ion for the enhancement of ionic conductivity of the composite solid electrolyte. This argument is in agreement with the previously reported study from the previous investigations where the Li^+ ion mobility could be promoted and enhanced at temperature of 252 °C whenever the long range and rigid order of crystalline $LiNO_3$ has been broke down [22].

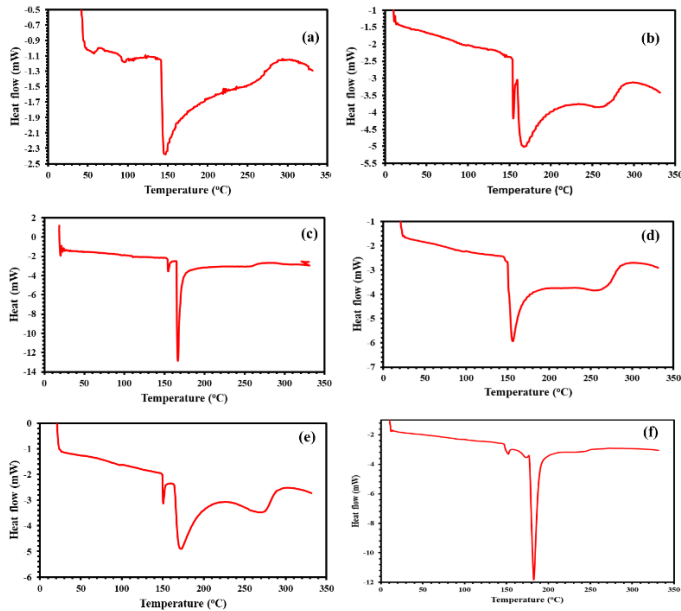


Figure 2: DSC curves of $(1-x)MgCO_3 - xAl_2O_3$ composites where x of (a) 0.2; (b) 0.7; (c) 0.6; (d) 0.5; (e) 0.4; (f) 0.9.

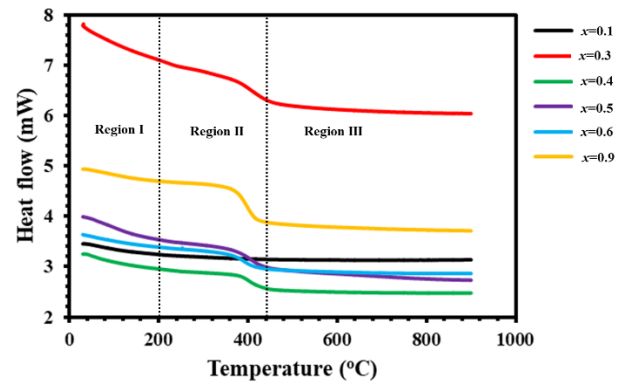


Figure 3: TGA curves of $(1-x)MgCO_3 - xAl_2O_3$ composites.

3.3 FTIR analysis

The chemical bonding of the as-prepared materials after calcination were determined by using FTIR as indicated in Figure 4. The chemical bonding of interest in the present investigations are the occurrence of $MgCO_3$, $Mg-O$, CO_3^{2-} and $Al-O$ bonds which can be divided into several distinct regions. The combination band appeared with a weaker strength at 2020 cm^{-1} in accordance to previously reported by Colomaban [27]. Whereas, the formation of asymmetric stretching vibration of carbonate anion from $MgCO_3$ can be observed between $1300 - 1500\text{ cm}^{-1}$ which is closed to Hu et al. [28]. Furthermore, the existence of $Al-O-Al$ bond in the as-prepared composite can be obtained at $1100 - 1150\text{ cm}^{-1}$ which is in parallel with other studies by Khazaei et al. [19] where they reported that the presence of $Al-O-Al$ bond took place in the wide region of $300 - 1000\text{ cm}^{-1}$. Another report by Potdar et al. [29] stating that the occurrence of $Al-O-Al$ bond could be obtained at 1073 cm^{-1} and a shoulder at 1163 cm^{-1} . Meanwhile, $Mg-O-Mg$ bond of MgO can be obtained from a weak intensity around 870 cm^{-1} [30, 31]. On the other hand, the formation of $Al-O$ stretching vibration also can be obtained at around 550 cm^{-1} which in agreement with Tong et al who reported that the $Al-O$ bond can be deduced between $900 - 500\text{ cm}^{-1}$ [32]. Additionally, the existence of $MgCO_3$ can be observed at wavenumber of around 420 cm^{-1} which is in accordance with BrusenTsova et al. [33] which is appeared in between $380 - 439\text{ cm}^{-1}$.

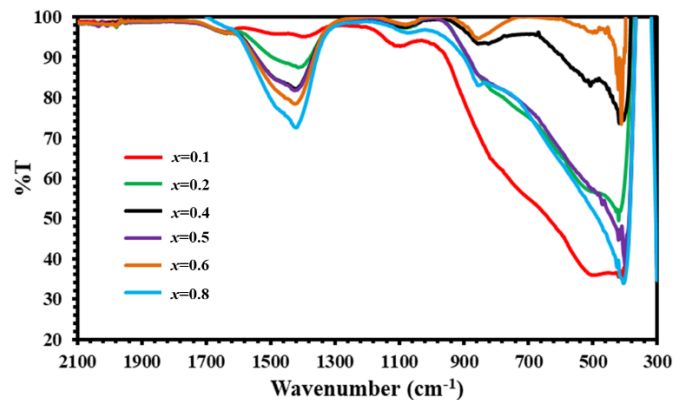


Figure 4: FTIR of $MgCO_3$ and $(1-x)MgCO_3 - xAl_2O_3$ composites.

3.4 FESEM-EDX analyses

Structural information of the as-prepared composites can be investigated by FESEM micrographs as indicated in Figure 5 below. The surface structure of the composite seems to form intense with spherical-like agglomeration and a lot of visible pores either on the surface or at the cross-section. The formation of agglomerated structure might provide better charge/discharge capacity due to excellent trap density that shortens the diffusion of Mg^{2+} ion [34, 35]. Moreover, calcination of the composite at such a high temperature would be able to reduce the electrical resistivity, induce Joule heating, producing more compact and dense structure of composite leading to possibility of higher conductivity [36]. In addition, the formation of all the expected elements namely Mg, Al and O can be found in good agreement between each other as indicated by EDS analysis from two different spots in Figure 6 which further confirm the uniform dispersion of MgO particles.

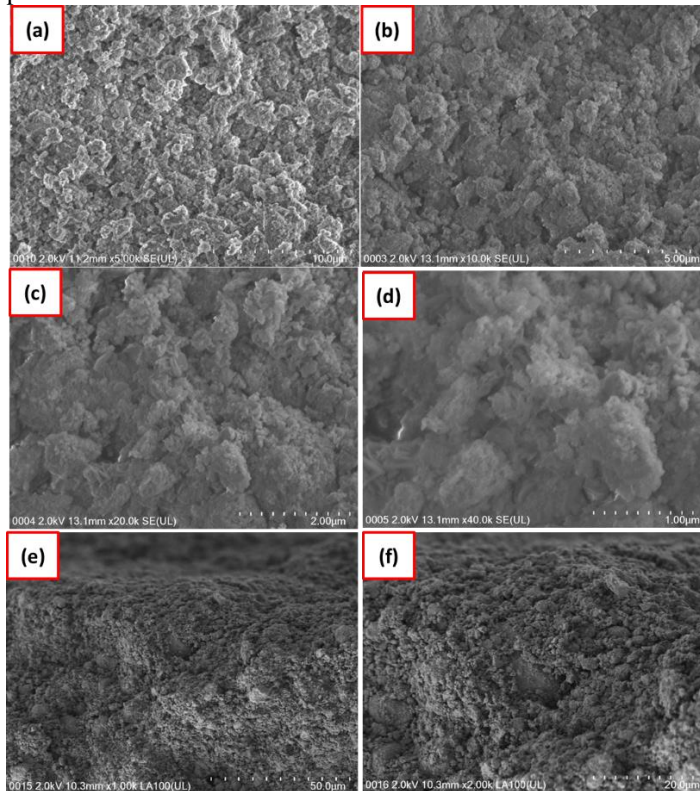


Figure 5: FESEM micrographs of $(1-x)MgCO_3-xAl_2O_3$ composites with $x = 0.9$. On the pellet surface (a – d); pellet cross-section (e – f).

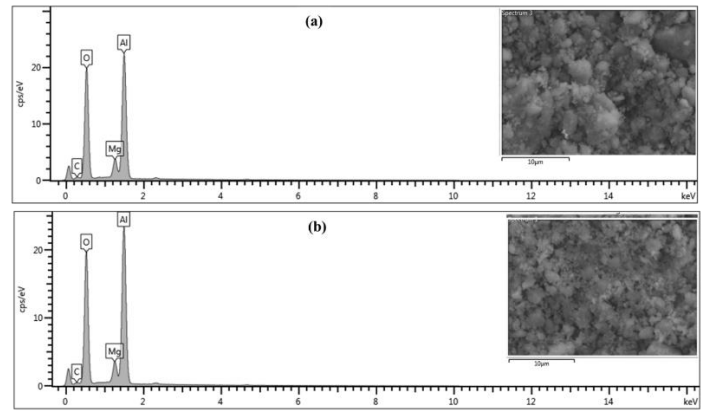


Figure 6: EDX spectra for $(1-x)MgCO_3-xAl_2O_3$ composites with $x = 0.9$.

3.5 Onductivity measurements

The electronic conductivity of the prepared composite was investigated through chronoamperometry method at 50 mV by investigating the current density as a function of time as indicated in Figure 7. The prepared material seems to be stable after the measurement although it underwent a sudden drop at the start of the measurement. The sudden decrease in current density at the beginning of the measurement ($t = 0s$) from $2.75 \mu A.cm^{-2}$ to $2.41 \mu A.cm^{-2}$ at $t = 2000s$ is due to over potential or polarization of the material involving the rearrangement of Mg^{2+} ions which is in agreement with recently reported studies by Mohammad et al. [37] and Nowak et al. [38]. Furthermore, the decrement in current to the steady state values also can be assigned owing to the growth of the passivation layer at the electrode and the accomplishment of salt concentration gradient in the prepared composites [39]. The electronic conductivity (σ_{el}) obtained for these materials for all ratios as indicated in Table 1 are in order of $10^{-6} S.cm^{-1}$ which is lower than the σ_{el} of metals and semiconductors, suggestive the electronic insulating behavior of these newly prepared composites [40, 41]. The electronic conductivity of the material can be obtained using the formula of $\sigma_{el} = j.d/U$ where σ_{el} is electronic conductivity, j is current density, d is diameter and U is the applied voltage [37]. Additionally, cationic transference number (t_{ion}) can be obtained from the formula of $t_{ion} = (I_T - I_R)/I_T$ where I_T and I_R is defined as total and residual current, respectively and it is decreased as the value of x increased or as the amount of alumina increased in the composites (Figure 8). From the author's point of view, as the amount of $MgCO_3$ increased in the composites, more ionic species of Mg^{2+} and CO_3^{2-} ions are produced from the dissociation reaction of $MgCO_3$ which could lead to agglomeration or forming new ionic cluster that could be able to block the transport of ions thus could lower the conductivity of the composites. Furthermore, instead of Mg^{2+} cations, CO_3^{2-} anions also play a significant role in governing the total conductivity of the prepared composites as previously reported by Zainuddin et al. [42]. Moreover, the involvement of anions towards the conductivity of the solid electrolyte can be further acquainted when the group of Nicotera reported that TFSI anions are more transportable than Li^+ ion from self-diffusion coefficient studies [43].

Typically, several factors contribute to the ionic conductivity of the electrolyte such as ionic mobility, charge carrier concentrations and ionic charges in which the

conductivity will be upsurge as the mobility of ions increases [44, 45]. From Figure 9, the ionic conductivity increased as the amount of alumina decreased or x values increased which give the highest conductivity value of 1.8×10^{-4} S.cm⁻² when $x = 0.9$. The decrement in conductivity of the composites as the amount of MgO increased might be due to blocking of conducting pathway of the ions when ionic dissociation processes is more dominant process than ionic association process [46]. Furthermore, addition of more MgO in the composites leads to the agglomeration of the ionic species producing new ionic clusters that could retard the mobility of the ions, thus contribute to the decreasing conductivity [47, 48]. In order to enhance the conductivity if the solid composite electrolyte, the concentration of defect in the space charge layer formed between MgO and Al₂O₃ should be taken into account. Taking the ratio of $x = 0.9$ as an example with the highest conductivity among other ratios, from the author's knowledge, the enhancement of conductivity followed the Maier's space charge model due to the presence of high defect concentration in the space charge region at the interface as a consequence of surface interaction between two different phases of MgO and Al₂O₃. Based on our previous publication [49], due to slightly electronegative behavior of MgO naturally, strong chemical adsorption of ions namely Mg²⁺ take place at the surface of MgO forming MgO-Mg²⁺ species [49, 50]. This process is a reversible process and the formation of MgO-Mg²⁺ species might be also due to the lattice distortion associated with local asymmetric electric field at the surface [49]. Meanwhile, the filler (dispersoid) which act as insulating oxide or support is regarded as hydroxyl group which is referred as nucleophile. The cationic species namely Mg²⁺ on the surface of MgO from MgO-Mg²⁺ species, will be attracted to this hydroxyl group at the interface of MgO-Al₂O₃. As a consequence, the interface of MgO-Al₂O₃ will be enriched by positively charged layer of Mg²⁺ and a layer of cationic vacancies which describe the surface disordering lead to the enhancement of defect concentration at the interface of MgO-Al₂O₃ which further increase the movement of Mg²⁺ ion and the conductivity of the composite [51]. The ionic conductivity (σ_{ion}) can be determined using the formula of $\sigma_{ion} = t/R_b A$ where t is referred to the thickness of the pellet, R_b is bulk resistance (Ω) and A is the area of the pellet (cm²).

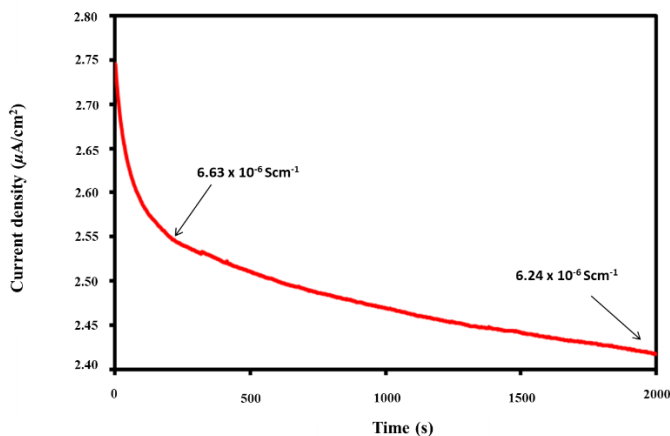


Figure 7: Chronoamperometry of $(1-x)\text{MgCO}_3-x\text{Al}_2\text{O}_3$ composites with at 30 °C (J versus time (s)) with $x = 0.9$.

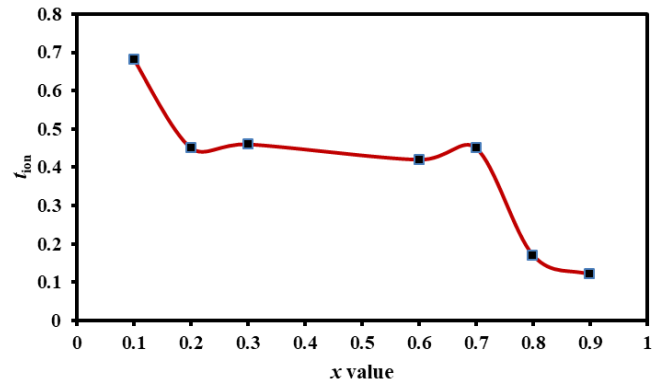


Figure 8: Transference number (t_{ion}) of $(1-x)\text{MgCO}_3-x\text{Al}_2\text{O}_3$ at room temperature with $x = 0.1 - 0.9$

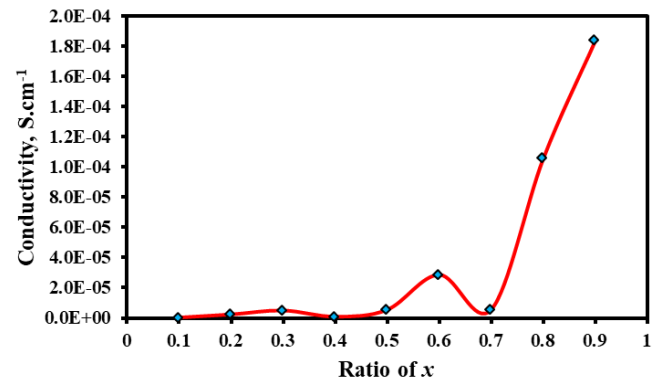


Figure 9: The ionic conductivity as a function of composition (x) for $(1-x)\text{MgCO}_3-x\text{Al}_2\text{O}_3$ at room temperature with $x = 0.1 - 0.9$.

Furthermore, Figure 10 showed an example of Nyquist impedance plot at 30 °C for the determination of ionic conductivity (σ_{ion}) of the material with $x = 0.9$. The Nyquist plots for other ratios show the same patterns. The impedance plot of composite which comprises a broad semicircle can be assigned as bulk properties of the material. The intercept of the semicircle at low frequency (right) with the real axis or Z' -axis give the information on the grain interior or bulk resistance (R_b) of the material [52]. Moreover, it is generally understood that the electrical resistivity will be decreased as the temperature increased. From Figure 11, the R_b values for example for $x = 0.7, 0.8$ and 0.9 ratio increased as the temperature increased up to certain temperature before going down as the temperature rises up. Other solid composite electrolytes have been reported to undergo the same phenomenon in lowering the electrical resistivity as the temperature increase due to increasing Joule heating, thus forming high dense pellet which could probably lead to higher conductivity [53, 54]. The temperature dependence of conductivity can be obtained by Arrhenius equation of $\sigma = A \exp(-E_a/RT)$ where A is the pre-exponential factor, E_a is the activation energy (eV) while k is the Boltzmann's constant with the value of 8.52×10^{-5} eV/K and T is the temperature (K). From Figure 12, the trends in conductivity for all ratios are the same where the conductivity started to decrease as the temperature more than 90 °C.

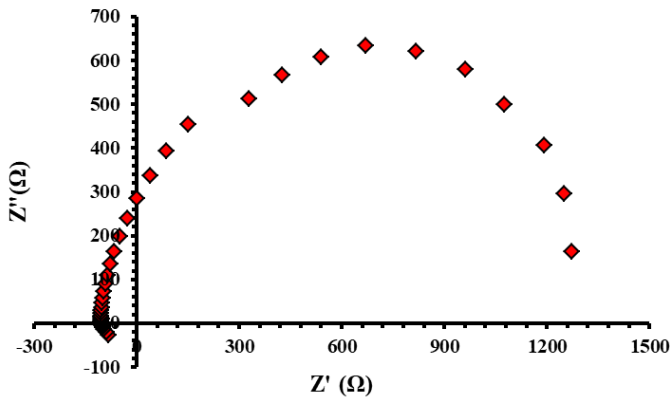


Figure 10: Complex impedance spectroscopy of $(1-x)\text{MgCO}_3-x\text{Al}_2\text{O}_3$ composites with $x = 0.9$.

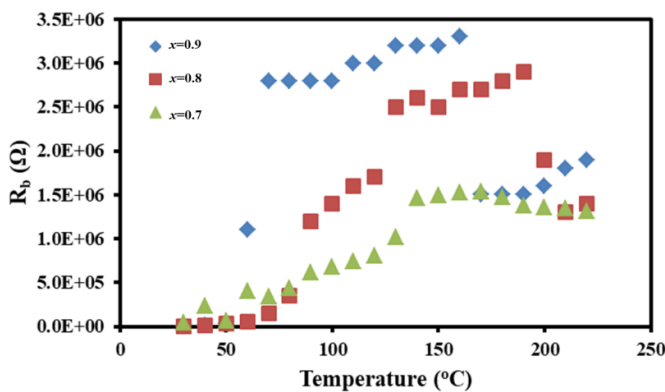


Figure 11: R_b values of $(1-x)\text{MgCO}_3-x\text{Al}_2\text{O}_3$ composites versus temperature with $x = 0.7, 0.8$ and 0.9 .

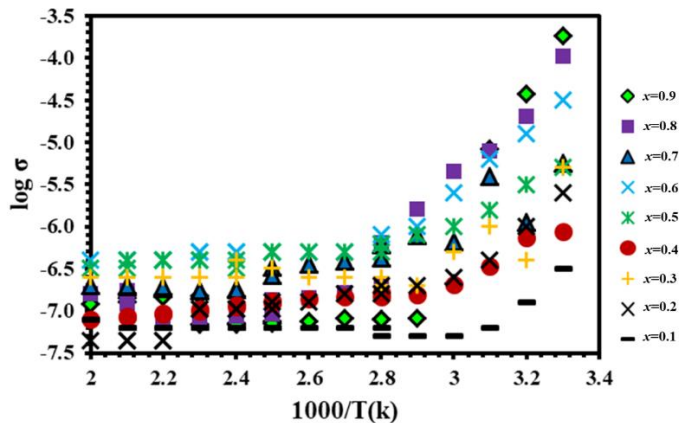


Figure 12: The ionic conductivity of $(1-x)\text{MgCO}_3-x\text{Al}_2\text{O}_3$ composites versus inverse of temperature with $x = 0.1 - 0.9$.

4. CONCLUSIONS

To conclude, for the first time the composite solid electrolyte of $(1-x)\text{MgCO}_3-x\text{Al}_2\text{O}_3$ with $x = 0.1 - 0.9$ by sol-gel method show the highest conductivity in order of $10^{-4} \text{ S.cm}^{-1}$. The highest conductivity of the composites in the present studies account for several factors such as, increasing amorphousness of the materials as the amount of Al_2O_3 in the composites increased, better interfacial contact between

MgCO_3 and Al_2O_3 and formation of MgO-Mg^{2+} species which govern the charge carriers transfer.

ACKNOWLEDGEMENT

The authors would like to thank the University of Malaya for granting the Research Grant (GPH005H2018) to support this work.

REFERENCES

- [1] J. Muldoon, C.B. Bucur, T. Gregory, Quest for nonaqueous multivalent secondary batteries: magnesium and beyond, *Chemical Reviews*, 114 (2014) 11683-11720.
- [2] P. Canepa, G. Sai Gautam, D.C. Hannah, R. Malik, M. Liu, K.G. Gallagher, K.A. Persson, G. Ceder, Odyssey of multivalent cathode materials: open questions and future challenges, *Chemical Reviews*, 117 (2017) 4287-4341.
- [3] C.B. Bucur, Challenges of a Rechargeable Magnesium Battery: A Guide to the Viability of this Post Lithium-Ion Battery, Springer 2017.
- [4] R. Attias, M. Salama, B. Hirsch, Y. Goffer, D. Aurbach, Anode-electrolyte interfaces in secondary magnesium batteries, *Joule*, 3 (2019) 27-52.
- [5] M. Sulaiman, N.C. Su, N. Mohamed, Sol-gel synthesis and characterization of $\beta\text{-MgSO}_4: \text{Mg}(\text{NO}_3)_2\text{-MgO}$ composite solid electrolyte, *Ionics*, 23 (2017) 443-452.
- [6] X. Yu, J. Bates, G. Jellison Jr, F. Hart, A stable thin-film lithium electrolyte: lithium phosphorus oxynitride, *Journal of the Electrochemical Society*, 144 (1997) 524.
- [7] J. Bates, N. Dudney, G. Gruzalski, R. Zuhur, A. Choudhury, C. Luck, J. Robertson, Electrical properties of amorphous lithium electrolyte thin films, *Solid state ionics*, 53 (1992) 647-654.
- [8] W. Li, C. Li, C. Zhou, H. Ma, J. Chen, Metallic magnesium nano/mesoscale structures: their shape-controlled preparation and Mg/air battery applications, *Angewandte Chemie International Edition*, 45 (2006) 6009-6012.
- [9] Y. Liu, L. Jiao, Q. Wu, J. Du, Y. Zhao, Y. Si, Y. Wang, H. Yuan, Sandwich-structured graphene-like MoS_2/C microspheres for rechargeable Mg batteries, *Journal of Materials Chemistry A*, 1 (2013) 5822-5826.
- [10] T. Wen, E. Jin, L. Yuan, J. Yu, Y. Zhou, C. Tian, Structure and ionic conductivity of $\text{ZrO}_2(\text{MgO})/\text{CaO-Al}_2\text{O}_3$ bilayer system used as solid electrolyte for sulfur sensor, *Materials Research Bulletin*, 117 (2019) 113-119.
- [11] Y. Jiang, Y. Zhou, Z. Hu, Y. Huang, X. Zhu, MgO or Al_2O_3 crucible: Which is better for the preparation of LLZ-based solid electrolytes?, *Ceramics International*, 46 (2020) 3367-3373.
- [12] Y. Mateyshina, A. Slobodyuk, V. Kavun, N. Uvarov, Conductivity and NMR study of composite solid electrolytes $\text{CsNO}_2\text{-A}$ ($\text{A} = \text{SiO}_2, \text{Al}_2\text{O}_3, \text{MgO}$), *Solid State Ionics*, 324 (2018) 196-201.
- [13] Z. Xia, B. Meng, H. Zhang, Q. Zheng, W. Liang, X. Ping, Effects of MgO additions on the electrical conduction behavior of a CeO_2 -based electrolyte prepared by SPS process, *Ceramics International*, 46 (2020) 9622-9628.
- [14] M. Sulaiman, A.A. Rahman, M. Nor Sabirin, $\text{Li}_2\text{CO}_3\text{-Al}_2\text{O}_3$ composite solid electrolytes prepared by sol gel method, *Key Engineering Materials*, Trans Tech Publ, 2011, pp. 379-384.
- [15] K.S. Alber, J.A. Cox, Electrochemistry in solids prepared by sol-gel processes, *Microchimica Acta*, 127 (1997) 131-147.

- [16] L. Fu, H. Liu, C. Li, Y. Wu, E. Rahm, R. Holze, H. Wu, Electrode materials for lithium secondary batteries prepared by sol–gel methods, *Progress in Materials Science*, 50 (2005) 881-928.
- [17] B. Ding, Z. Ahsan, X. Huang, Z. Cai, Y. Ma, G. Song, W. Yang, C. Wen, Preparation and electrochemical properties of high capacity silicon-based composites for lithium-ion batteries, *Synthetic Metals*, 261 (2020) 116324.
- [18] M.Z. Iqbal, Enhanced ionic conduction of CdI₂-Ag₂-CrO₄ and Al₂O₃ composite solid electrolytes, *Current Applied Physics*, 16 (2016) 974-979.
- [19] S. Nazari, G. Karimi, E. Ghaderi, K. Mansouri Moradian, Z. Bagherpor, Synthesis and characterization of γ -alumina porous nanoparticles from sodium aluminate liquor with two different surfactants, *International Journal of Nanoscience and Nanotechnology*, 12 (2016) 207-214.
- [20] M. Urbonavicius, S. Varnagiris, L. Pranevicius, D. Milcius, Production of gamma alumina using plasma-treated aluminum and water reaction by products, *Materials*, 13 (2020) 1300.
- [21] N. Uvarov, Composite solid electrolytes: recent advances and design strategies, *Journal of Solid State Electrochemistry*, 15 (2011) 367-389.
- [22] M. Sulaiman, A. Rahman, N. Mohamed, Effect of water-based sol gel method on structural, thermal and conductivity properties of LiNO₃–Al₂O₃ composite solid electrolytes, *Arabian Journal of Chemistry*, 10 (2017) 1147-1152.
- [23] F. Croce, G. Appetecchi, L. Persi, B. Scrosati, Nanocomposite polymer electrolytes for lithium batteries, *Nature*, 394 (1998) 456-458.
- [24] P.N. Joge, D. Kanchan, P.L. Sharma, Effect of Al₂O₃ on crystallinity and conductivity of PVA–PEO–EC–LiCF₃SO₃ blend electrolyte system, *AIP Conference Proceedings*, American Institute of Physics, 2014, pp. 356-357.
- [25] Y. Oikawa, T. Saito, S. Idomukai, T. Tanaka, M. Nishida, H. Sawada, Preparation of magnesium carbonate nanoparticles encapsulated by nanocomposite material derived from fluoroalkyl end-capped vinyltrimethoxysilane oligomer–Application to the surface modification of glass and poly(methyl methacrylate), *Journal of Fluorine Chemistry*, 177 (2015) 70-79.
- [26] A.R. Polu, R. Kumar, Preparation and characterization of PEG–Mg(CH₃COO)₂–CeO₂ composite polymer electrolytes for battery application, *Bulletin of Materials Science*, 37 (2014) 309-314.
- [27] P. Colomban, Raman study of the formation of transition alumina single crystal from protonic β/β' "aluminas, *Journal of Materials Science Letters*, 7 (1988) 1324-1326.
- [28] X.-y. Hu, Q.-y. Liu, M.-x. Jing, F. Chen, B.-w. Ju, F.-y. Tu, X.-q. Shen, S.-b. Qin, Controllable preparation of alumina nanorods with improved solid electrolyte electrochemical performance, *Ceramics International*, (2020).
- [29] H.S. Potdar, K.-W. Jun, J.W. Bae, S.-M. Kim, Y.-J. Lee, Synthesis of nano-sized porous γ -alumina powder via a precipitation/digestion route, *Applied Catalysis A: General*, 321 (2007) 109-116.
- [30] N. Zeeshan, Solid electrolytes based on $\{1-(x+y)\}$ ZrO₂-(x)MgO-(y)CaO ternary system: Preparation, characterization, ionic conductivity, and dielectric properties, *Journal of Advanced Research*, 9 (2018) 35-41.
- [31] M.-R. Song, M. Chen, Z.-J. Zhang, Preparation and characterization of Mg nanoparticles, *Materials Characterization*, 59 (2008) 514-518.
- [32] Y. Tong, J. Wirth, H. Kirsch, M. Wolf, P. Saalfrank, R.K. Campen, Optically probing Al–O and O–H vibrations to characterize water adsorption and surface reconstruction on α -alumina: An experimental and theoretical study, *The Journal of Chemical Physics*, 142 (2015) 054704.
- [33] T.N. Brusentsova, R.E. Peale, D. Maukonen, G.E. Harlow, J.S. Boesenberg, D. Ebel, Far infrared spectroscopy of carbonate minerals, *American Mineralogist*, 95 (2010) 1515-1522.
- [34] H. Deng, I. Belharouak, Y.-K. Sun, K. Amine, Li_xNi_{0.25}Mn_{0.75}O_y (0.5 ≤ x ≤ 2, 2 ≤ y ≤ 2.75) compounds for high-energy lithium-ion batteries, *Journal of Materials Chemistry*, 19 (2009) 4510-4516.
- [35] A. Kumar, R. Nazzario, L. Torres-Castro, A. Pena-Duarte, M. Tomar, Electrochemical properties of MgO-coated 0.5Li₂MnO₃-0.5LiNi_{0.5}Mn_{0.5}O₂ composite cathode material for lithium ion battery, *International Journal of Hydrogen Energy*, 40 (2015) 4931-4935.
- [36] M. S Medina, S. GM Carvalho, E. NS Muccillo, R. Muccillo, Enhancement of the ionic conductivity in electric field-assisted pressureless sintered BITIVOX solid electrolytes, *Ceramics*, 2 (2019) 502-513.
- [37] I. Mohammad, J. Chable, R. Witter, M. Fichtner, M.A. Reddy, Synthesis of Fast Fluoride-Ion-Conductive Fluorite-Type Ba_{1-x}Sb_xF_{2+x} (0.1 ≤ x ≤ 0.4): A Potential Solid Electrolyte for Fluoride-Ion Batteries, *ACS Applied Materials & Interfaces*, 10 (2018) 17249-17256.
- [38] S. Nowak, F. Berkemeier, G. Schmitz, Ultra-thin LiPON films–Fundamental properties and application in solid state thin film model batteries, *Journal of Power Sources*, 275 (2015) 144-150.
- [39] A.M. Sureshini, A. Nishimoto, M. Watanabe, Transport and electrochemical characterization of plasticized poly (vinyl chloride) solid electrolytes, *Solid State Ionics*, 86 (1996) 385-393.
- [40] R.A. Matula, Electrical resistivity of copper, gold, palladium, and silver, *Journal of Physical and Chemical Reference Data*, 8 (1979) 1147-1298.
- [41] Y. Wang, L. Wang, K.-c. Chou, Estimating electrical conductivities of CaO–MgO–Al₂O₃–SiO₂ using ion-oxygen parameter, *High Temperature Materials and Processes*, 35 (2016) 253-259.
- [42] Z. Zainuddin, D. Hambali, I. Supa'at, Z. Osman, Ionic conductivity, ionic transport and electrochemical characterizations of plastic crystal polymer electrolytes, *Ionics*, 23 (2017) 265-273.
- [43] I. Nicotera, C. Oliviero, W.A. Henderson, G.B. Appetecchi, S. Passerini, NMR Investigation of Ionic Liquid–LiX Mixtures: Pyrrolidinium Cations and TFSI- Anions, *The Journal of Physical Chemistry B*, 109 (2005) 22814-22819.
- [44] A. Arof, S. Amirudin, S. Yusof, I. Noor, A method based on impedance spectroscopy to determine transport properties of polymer electrolytes, *Physical Chemistry Chemical Physics*, 16 (2014) 1856-1867.
- [45] W. Chong, Z. Osman, The effect of carbonate-phthalate plasticizers on structural, morphological and electrical properties of polyacrylonitrile-based solid polymer electrolytes, *Journal of Polymer Research*, 21 (2014) 381.
- [46] N. Kaus, A. Ahmad, Conductivity studies and ion transport mechanism in LiI–Li₃PO₄ solid electrolyte, *Ionics*, 15 (2009) 197-201.
- [47] C.V.S. Reddy, X. Han, Q.-Y. Zhu, L.-Q. Mai, W. Chen, Conductivity and discharge characteristics of (PVC+ NaClO₄)

polymer electrolyte systems, *European Polymer Journal*, 42 (2006) 3114-3120.

[48] L. Othman, K.B.M. Isa, Z. Osman, R. Yahya, Ionic conductivity, morphology and transport number of lithium ions in PMMA based gel polymer electrolytes, *Defect and Diffusion Forum*, Trans Tech Publ, 2013, pp. 137-142.

[49] M. Sulaiman, A. Rahman, N. Mohamed, Structural, thermal and conductivity studies of magnesium nitrate–alumina composite solid electrolytes prepared via sol-gel method, *Int. J. Electrochem. Sci.*, 8 (2013) 6647-6655.

[50] J. Maier, Defect chemistry and conductivity effects in heterogeneous solid electrolytes, *Journal of The Electrochemical Society*, 134 (1987) 1524.

[51] N.F. Uvarov, V. Ponomareva, G. Lavrova, Composite solid electrolytes, *Russian Journal of Electrochemistry*, 46 (2010) 722-733.

[52] S.B. Aziz, M. Hamsan, R.M. Abdullah, M. Kadir, A promising polymer blend electrolytes based on chitosan: methyl cellulose for EDLC application with high specific capacitance and energy density, *Molecules*, 24 (2019) 2503.

[53] M. S. Medina, S. G.M. Carvalho, E. N.S. Muccillo, R. M., Enhancement of the ionic conductivity in electric field-assisted pressureless sintered BITIVOX solid electrolytes, *Ceramics*, 2 (2019) 502-513.

[54] B. Singh, S. Ghosh, S. Aich, B. Roy, Low temperature solid oxide electrolytes (LT-SOE): A review, *Journal of Power Sources*, 339 (2017) 103-135.